



Boundary Effect Reduction in Image Filtering

Yong Ge^{1,2}, Qiuming Cheng²

*1 State Key Laboratory of Resources and Environmental Information System,
Institute of Geographic Sciences & Natural Resources Research, Chinese Academy of Sciences
A 11 Datun Rd., Beijing 100101, China.*

Email: gey@lreis.ac.cn; Tel: 8610 64888967; Fax: 8610 64889630.

*2 Department of Earth and Space Science and Engineering, York University
4700 Keele St., Toronto, ON, Canada, M3J 1P3.*

Abstract

The abrupt boundary truncation of an image may cause bright strips on a 2-D power spectrum in frequency domain and distortion of patterns in the frequency domain. The traditional solutions, including zero-padding and extension of the image by mirroring the data inside image, are useable for processing relatively simple, regular and stationary images. These methods, however, are not effective for dealing with images with holes or highly irregular shapes. This paper proposes an algorithm of using decay functions to handle boundary effects especially when filtering operation is involved in image processing. To validate the algorithm, we first employ a geochemical image interpolated by data set from a mineral district in Nova Scotia, Canada to analyze the effects of decay function on boundary truncations with the change of extension width. We then apply the algorithm to a real-life remotely sensed image. It is demonstrated that decay functions give superior overall performances over the traditional method.

Keywords: *Boundary effect; Decay functions; Image processing.*

1. Introduction

Filtering an image, suppressing certain information while leaving others unchanged on the image [1], is one of the most important techniques for information extraction from the image. However, the filtering analysis is often complicated by so called boundary effects caused by sharp intensity differences on the image boundaries and the boundaries of holes within the study area. The noise due to the boundary effect will lead to the roughness of density estimates increasing towards the boundaries of a study region as the effective size of the filter decreases in spatial filtering, bring about a distortion of the spectrum in frequency filtering operation [2] and produce false information and affect subsequent operations [3~5]. Over recent years, the issue of eliminating the boundary effect has been taken substantial efforts and

some excellent techniques developed by researchers[1],[6~10]. Woods (1995) was the first to discuss the boundary truncation artifact. Tan et al. (1991) have discussed the boundary artifacts and proposed optimal window techniques. Later, the well-known zero-padding method that smoothes the boundary to zeros using the zero-padding method has been accepted as common solutions to eliminate the boundary effect [1]. This method improves the filtering results but still leave with some distortions especially along the edges. Subsequently, Aghdasi and Ward (1996) proposed a method to smooth the edge by reflecting the original image to extend the image. This method improved the result further. Though the proceeding methods are applicable for situations where images have regular shapes, they are not effective for dealing with images with holes or highly irregular shapes such as remotely sensed images with irregular mask and the images interpolated from the values of these samples from unevenly distributed samples covering an irregular area of the Earth's surface. If we use the traditional methods to deal with these images, it may still leave a new boundary truncation at the irregular boundaries of image and holes within image. The noise caused by the new boundary truncation may still affect the patterns of spectrum, especially high-pass filtering operation in frequency domain where most of noise caused by boundary effect will be mistakenly identified as useful information.

Compared to traditional methods, this algorithm smoothed the boundaries of the image with aid of decay functions and it showed overall superior results in the reduction of boundary effects. In this paper we mainly discussed the implementation of the reduction of boundary effect using decay functions. It is useful for readers who want to repeat this algorithm to deal with their data.

In section 2, a basic idea of the algorithm will be given. Sections 3 and 4 describe two experiments to show how to use this method with real life data. In



section 5, we conclude the paper with a summary and outlook for further research.

2. Description of Algorithm

2.1 Filtering in Frequency Domain

Consider an input image $f(x, y)$ of size $M \times N$, $0 \leq x \leq M-1$, $0 \leq y \leq N-1$. The discrete Fourier transform (DFT) of $f(x, y)$ is given by the equation

$$F(u, v) = \frac{1}{MN} \sum_{x=0}^{M-1} \sum_{y=0}^{N-1} \exp(-2\pi i u x / M) \exp(-2\pi i v y / N) f(x, y) \\ = \text{DFT}(f(x, y))$$

$$f(x, y) = \sum_{u=0}^{M-1} \sum_{v=0}^{N-1} \exp(2\pi i u x / M) \exp(2\pi i v y / N) F(u, v) \\ = \text{DFT}^{-1}(F(u, v))$$

(1)

$$S(u, v) = |F(u, v)|^2 = R^2(u, v) + I^2(u, v)$$

$$g(x, y) = \text{DFT}^{-1}(H(u, v)F(u, v))$$

where $g(x, y)$ is obtained by means of the inverse discrete Fourier transform (DFT^{-1}), x and y are the image coordinates; $S(u, v)$ is the power spectrum, u and v are the wave numbers; $R(u, v)$ and $I(u, v)$ are the real and imaginary parts of $F(u, v)$, respectively. The term spectral density is also commonly used to denote the power spectrum [1]. $g(x, y)$, as a result image, is expressed as the convolution of Fourier transform function $F(u, v)$ and a filtering function $H(u, v)$. The filtering function can be defined according to the research objective. In Figure 1, we give the basic steps for reducing edge effects in Image Filtering in Frequency Domain.

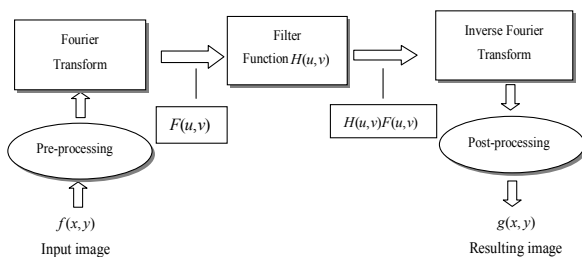


Figure 1. Basic steps for reducing boundary effects.

2.2 Boundary Effects Reduction Using Decay Functions

Two-dimensional image firstly is extended around its boundaries and within holes to a predetermined width, and then the extended portions of the image are filled with values calculated from decay function.

After extension to specified width Δ in an input image two-dimensional array $f(x, y)$ of size $M \times N$, the array of image becomes a new array $f^*(x, y)$ with

$$\text{size} \quad (M + 2\Delta) \times (N + 2\Delta) \\ -\Delta \leq x \leq M + \Delta - 1, -\Delta \leq y \leq N + \Delta - 1. \\ f^*(x, y) = \begin{cases} f(x, y) & \text{if } 0 \leq x < M, 0 \leq y < N \\ & \text{and } f(x, y) \neq \text{missing data} \\ f^{pad}(x, y) & \text{the padded value} \end{cases} \quad (2)$$

where let $f^{pad}(x, y) = 0$, we call this the zero-padding method for reducing the boundary effect [1].

2.2.1 Determination and Selection of Decay Functions

However, due to zero-padding and other traditional methods lack of capability for eliminating the boundary effects caused by irregular shapes and holes, decay functions are used to fill in the image extension and holes for areas of missing data. The decay functions we have investigated include linear, exponential and hyperbolic decay functions:

$$f^{pad}(x, y) = \begin{cases} f^{linear-decay}(x, y) \\ = (1 - \frac{\Delta_m}{\Delta}) f_0 \\ f^{exp-decay}(x, y) \\ = e^{-\lambda \Delta_m} f_0 \\ f^{hyper-decay}(x, y) \\ = (1 - (\frac{\Delta_m}{\Delta})^2)^2 f_0 \end{cases} \quad (3)$$

where $\lambda = (\ln f_0 - \ln \delta) / \Delta, 0 < \delta \ll 1$, f_0 represents the value at the boundary, Δ is an extended width, and $\Delta_m (\Delta_m < \Delta)$ represents distance from boundary point. From the above equations, we can see that different decay function will bring different effects on the reduction of boundary effects. It is therefore an important issue to decide how to select the appropriate decay function for padding the extended area. When the extended width is large and the boundary value is large, one can select the hyperbolic function because it can avoid new abrupt truncation of extended values to be produced. When the extension width is small and the boundary value is large, it is better to select the exponential function as decay function. The linear function is more suitable for selection when the extension width is not very small and the boundary value is not very large.

2.2.2 Determining the Status of Points at Boundaries

Before padding the extension area using decay functions, one needs to judge the status of points at boundaries and determine the category of pixel in the image because different types of pixels need different methods of padding. As illustrations in Figure 2, the irregular image generally consists of 5 different types of pixels: (1) pixels with meaningful values within the image (like point A); (2) pixels with bad values (missing data) (like point B); (3) pixels with meaningful values on the boundary of image (like point C); (4) pixels with meaningful values on the boundary of holes (like point D) and (5) isolated pixels with meaningful values (like point E). If a



point (like point B) falls in a hole, we consider this point as representing missing data. This case will not be analyzed further in this paper because by assigning the point a numerical value such as -9999 it can be easily identified as missing data.

After ascertaining the type a pixel belongs to, what we do next is to judge where this pixel is situated, that is, at the left boundary/boundary of image/hole, the right boundary/boundary of image/hole, the upper boundary/boundary of image/hole or at the bottom boundary/boundary of image/hole. For convenient understanding, we provide an approach to judge the status of a point along x coordinate. Similarly, we can

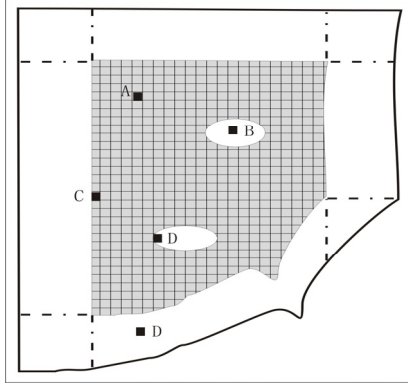


Figure 2. Five different types of pixel: (1) pixels with meaningful values lying within image (point A); (2) pixels with bad value (missing data) (point B); (3) pixels with meaningful values on the boundary of image (point C); (4) pixels with meaningful values on the boundary of hole (point D) and (5) isolated pixels with meaningful values (point E).

deal with points along y coordinate using this algorithm.

Suppose $x_B(1)$ and $x_B(2)$ are values of left bottom and right bottom of array of image along x coordinate; $y_B(1)$ and $y_B(2)$ are values of left bottom and left upper of array of image along y coordinate. Let MissingData be -9999. Variables Rows and Cols are numbers of rows and columns from the left bottom corner along with x, y coordinates respectively. Point $(Rows, Cols)$, also denoted $f_0(Rows, Cols)$ in equation 3, is a point to be judged. In Equation 4, we give the algorithm of judging the status of a pixel.

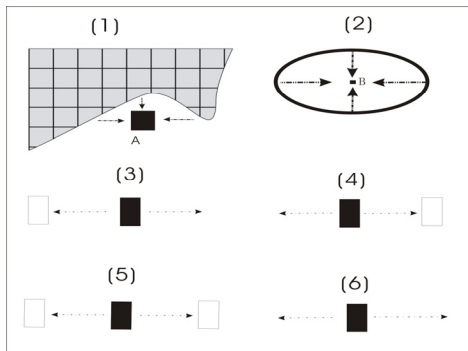


Figure 3. Pixel status.

```

1  If  $f_0(Rows, Cols) = \text{Missing Data}$ 
    Then it does not need treatment
2  (If  $x_B(1) < Rows < x_B(2)$  AND  $f_0(Rows, Cols) =$ 
    = Missing Data AND  $f_0(Rows - 1, Cols) =$ 
    Missing Data) OR (If  $y_B(1) < Cols < y_B(2)$  AND
     $f_0(Rows, Cols + 1) = \text{Missing Data}$  AND
     $f_0(Rows, Cols - 1) = \text{Missing Data}$ )
    Then Pixel is isolated data
3  If Rows =  $x_B(1)$ 
    Then Pixel on left boundary of image
4  If Rows =  $x_B(2)$ 
    Then Pixel on right boundary of image
5  If Cols =  $y_B(1)$ 
    Then Pixel on bottom boundary of image
6  If Cols =  $y_B(2)$ 
    Then Pixel on upper boundary of image
7  If  $x_B(1) < Rows < x_B(2)$  AND  $f_0(Rows + 1, Cols) =$ 
    = Missing Data AND  $f_0(Rows - 1, Cols) =$ 
    Missing Data
    Then Pixel on right boundary of hole
8  If  $x_B(1) < Rows < x_B(2)$  AND  $f_0(Rows + 1, Cols) =$ 
    Missing Data AND  $f_0(Rows - 1, Cols) =$ 
    Missing Data
    Then Pixel on right boundary of hole
9  If  $y_B(1) < Cols < y_B(2)$  AND  $f_0(Rows, Cols + 1) =$ 
    = Missing Data AND  $f_0(Rows, Cols - 1) =$ 
    Missing Data
    Then Pixel on bottom boundary of hole
10 If  $y_B(1) < Cols < y_B(2)$  AND  $f_0(Rows, Cols + 1) =$ 
    Missing Data AND
     $f_0(Rows, Cols - 1) = \text{Missing Data}$ 
    Then Pixel on upper boundary of hole
11 If Other
    Then Pixel is interior of image or others
    
```

(1) Pixel on Image Boundary

If Judge_Point equals 3, 4, 5 or 6, then pixel should lie on the boundary of image. Suppose we choose hyperbolic decay function here, then the padded value at any point that is within the extended width in the input image can be expressed as follows

$$f^{pad}(x, y) = \begin{cases} (1 - (\frac{\Delta_L}{\Delta})^2)^2 f_0(Rows, Cols) & \text{If Judge_Point } t = 3 \\ (1 - (\frac{\Delta_R}{\Delta})^2)^2 f_0(Rows, Cols) & \text{If Judge_Point } t = 4 \\ (1 - (\frac{\Delta_B}{\Delta})^2)^2 f_0(Rows, Cols) & \text{If Judge_Point } t = 5 \\ (1 - (\frac{\Delta_U}{\Delta})^2)^2 f_0(Rows, Cols) & \text{If Judge_Point } t = 6 \end{cases} \quad (5)$$

where $f_0(Rows, Cols)$ is boundary pixel; (x, y) is a point to be padded, Δ is an extended width; Δ_L means the distance between pixel on the left boundary of image and $f_0(Rows, Cols)$, Δ_R means the distance between pixel on the right boundary of image and $f_0(Rows, Cols)$, Δ_U means the distance between pixel on the upper boundary of image and $f_0(Rows, Cols)$, and Δ_B means the distance between pixel on the bottom boundary of image and $f_0(Rows, Cols)$ respectively.



Due to the irregular shape of an image and the holes within it, a location to be padded as seen in case 1 of Figure 3 may be calculated twice in two different directions. In that situation, we choose the average of the padded values as the final padded value. This treatment ensures the padded value is continuous at the join point. It may still leave an irregularity but the overall boundary effect is minimized.

(2) Pixel on Boundary of Hole

If Judge_Point equals 7, 8, 9 or 10, then pixel should lie on the boundary of hole. As before, we choose hyperbolic decay function here. The expression is almost the same as equation (5). The difference is that, in most cases, the point within hole will be calculated more than twice.

$$f^{pad}(x, y) = \begin{cases} (1 - (\frac{\Delta_L}{\Delta})^2)^2 f_0(Rows, Cols) & \text{If Judge_Point} = 7 \\ (1 - (\frac{\Delta_R}{\Delta})^2)^2 f_0(Rows, Cols) & \text{If Judge_Point} = 8 \\ (1 - (\frac{\Delta_B}{\Delta})^2)^2 f_0(Rows, Cols) & \text{If Judge_Point} = 9 \\ (1 - (\frac{\Delta_U}{\Delta})^2)^2 f_0(Rows, Cols) & \text{If Judge_Point} = 10 \end{cases} \quad (6)$$

where $\Delta_L, \Delta_R, \Delta_U$ and Δ_B have the same meaning as in equation (5).

If the width of hole is smaller than Δ , a point within a hole may be padded four times from four different directions as seen in case 2 of Figure 3. Each direction has its corresponding padded value. For the same reason as mentioned above, the final padded value is obtained by averaging these four values. If the width of hole is much greater than Δ , it is possible that the middle part with missing data left within the hole becomes a new hole. However, this new hole may not create many more boundary effects, because the boundary values are either zero or equal to small positive value δ much less than 1 if exponential decay function is used.

(3) Isolated Pixel

If Judge_Point equals 2, then pixel should be isolated pixel. In this case, we need to judge the status of pixel further. In Figure 3 (cases 3, 4, 5 and 6), we describe four types of status a pixel may be in.

(I): If there is no other pixel to the right of this pixel except missing data between itself and the very right of image and there is another pixel between itself and the very left of image, we define this pixel as *the first status* (case 3 in figure 3). The treatment then is as follows: assume the isolated point denotes $f_0(Rows, Cols)$ and another point to the left of this isolated point denotes $f_1(Rows1, Cols1)$.

$$f^{pad}(x, y) = \begin{cases} (1 - (\frac{\Delta_{right}}{\Delta})^2)^2 f_0(Rows, Cols) & \text{If } x > Rows \\ ((1 - (\frac{\Delta_{left}}{\Delta})^2)^2 f_0(Rows, Cols) + (1 - (\frac{\Delta_{right1}}{\Delta})^2)^2 f_1(Rows1, Cols1)) / 2 & \text{If } Rows1 < x < Rows \end{cases}$$

where Δ_{left} is the distance between point (x, y) and $f_0(Rows, Cols)$, and point (x, y) is to the left of $f_0(Rows, Cols)$ along x coordinate; Δ_{right} is the distance between point (x, y) and $f_0(Rows, Cols)$, and point (x, y) is to the right $f_0(Rows, Cols)$ along x coordinate; Δ_{right1} is the distance between point (x, y) and $f_1(Rows1, Cols1)$, and point (x, y) is to the right of $f_1(Rows1, Cols1)$ along x coordinate.

(II): If there is no other pixel to the left of this pixel except missing data between itself and the very left of image and there is another pixel to the right of this pixel between itself and the very right of image, we define this pixel as *the second status* (case 4 in figure 3). The treatment then is as follows: assume the isolated point denotes $f_0(Rows, Cols)$ and another point to the right of the isolated point denotes $f_1(Rows1, Cols1)$.

$$f^{pad}(x, y) = \begin{cases} (1 - (\frac{\Delta_{left}}{\Delta})^2)^2 f_0(Rows, Cols) & \text{If } x < Rows \\ ((1 - (\frac{\Delta_{right}}{\Delta})^2)^2 f_0(Rows, Cols) + (1 - (\frac{\Delta_{left1}}{\Delta})^2)^2 f_1(Rows1, Cols1)) / 2 & \text{If } Rows < x < Rows1 \end{cases}$$

where Δ_{left1} is the distance between point (x, y) and $f_1(Rows1, Cols1)$, and point (x, y) is to the left of $f_1(Rows1, Cols1)$ along x coordinate.

(III): If there is another pixel to the left of this pixel between and the very left of image and there is another pixel to the right of this pixel between and the very right of image, we define this pixel as *the third status* (case 5 in figure 3). The treatment then is as follows: Assume the isolated point denotes $f_0(Rows, Cols)$, the point to the right of the isolated point denotes $f_1(Rows1, Cols1)$ and the point to the left of the isolated point denotes $f_2(Rows2, Cols2)$.

$$f^{pad}(x, y) = \begin{cases} ((1 - (\frac{\Delta_{left}}{\Delta})^2)^2 f_0(Rows, Cols) + (1 - (\frac{\Delta_{right1}}{\Delta})^2)^2 f_1(Rows1, Cols1)) / 2 & \text{If } Rows1 < x < Rows \\ ((1 - (\frac{\Delta_{right}}{\Delta})^2)^2 f_0(Rows, Cols) + (1 - (\frac{\Delta_{left2}}{\Delta})^2)^2 f_2(Rows2, Cols2)) / 2 & \text{If } Rows < x < Rows2 \end{cases}$$

where Δ_{right1} is the distance between point (x, y) and



$f_1(Rows1, Cols1)$, and point (x, y) is to the right of $f_1(Rows1, Cols1)$ along x coordinate; Δ_{left2} is the distance between point (x, y) and $f_2(Rows2, Cols2)$, and point (x, y) is to the left of $f_2(Rows2, Cols2)$ along x coordinate.

(IV): If there is no other pixel to the left of this pixel between and the very left of image and there is no other pixel on the right of this pixel between itself and the right of image, we define this pixel as *the fourth status* (case 6 in figure 3). The point to be padded is treated as follows:

$$f^{pad}(x, y) = \begin{cases} (1 - (\frac{\Delta_{left}}{\Delta})^2)^2 f_0(Rows, Cols) & \text{If } x < Rows \\ (1 - (\frac{\Delta_{right}}{\Delta})^2)^2 f_0(Rows, Cols) & \text{If } x > Rows \end{cases}$$

where Δ_{left} is the distance between point (x, y) and $f_0(Rows, Cols)$, and point (x, y) is to the left of $f_0(Rows, Cols)$ along x coordinate; Δ_{right} is the distance between point (x, y) and $f_0(Rows, Cols)$, and point (x, y) is to the right $f_0(Rows, Cols)$ along x coordinate;

2.2.3 Padding Irregular Image using Decay Functions

Based on the proceeding treatment, we can obtain an extended image $f^*(x, y)$ (as described in equation 2) which has new boundary values close to zero. If the image has a regular shape, then the padded surface is smooth. Otherwise, if the shape is irregular, at sharp corners and within small holes some discontinuities can still be expected and these may cause boundary effects. Because these locations at sharp corners and other discontinuities do not usually occupy a large portion of the image, the preceding treatment usually provides satisfactory results. One of advantages of this method is that one can view the extended image prior to application of the Fourier transform and get some idea of how much smoothness the treatment has added to the image. This can help one to decide how large the extended image portion (Δ) should be. An alternative treatment would be to expand the image during the calculation of the integral of the Fourier transform. From a programming point of view, the treatment described in here can be added independently without altering the Fourier transform and inverse Fourier transform steps in processing.

2.2.4 Obtaining the Resulting Image Using the Algorithm

Given the expanded image $f^*(x, y)$, we can apply the Fourier transform (F^*) to calculate the power spectrum (S^*) and to define filter functions (H) (in this paper, a multifractal filtering function was

defined the filter). Then the resulting image $g(x, y)$ of size $M \times N$, $0 \leq x \leq M - 1$ can be clipped from $DFT^{-1}(H(u, v)F^*(u, v))$ with dimension $(M + 2\Delta) \times (N + 2\Delta)$.

3. Case One: A Geochemical Image

For validating the proceeding argument, here we first chose a lake sediment geochemical data from Nova Scotia, Canada.

3.1 Study Area

The study area is located in western Meguma Terrain of Nova Scotia, Canada. The map created from the lake sediment sample point values has a dimension of 359 x 425 and cell size 500m.

3.2 Defining the Filtering Function

There are various ways to define $H(u, v)$. For example, simple low-pass filter, high-pass filter and band-pass filter commonly are constructed on the basis of ranges of frequencies. We here choose a multifractal filter which is called spectrum-area fractal method (S-A) for separating geochemical anomalies from background patterns. The S-A method, which has been implemented in GeoDAS (GeoData Analysis System, a GIS software system developed by the Geomatics Research Group at York University, Canada, in collaboration with the Geological Survey of Canada and US Geological Survey, is a newly developed filtering method that has been successfully used for processing geochemical patterns with anisotropic and singular properties [11],[12].

The S-A method defines filter functions on the basis of power spectrum levels as follows:

$$H_B(u, v) = \begin{cases} 1 & \text{if } S(u, v) > S_0 \\ 0 & \text{otherwise} \end{cases}$$

$$H_A(u, v) = \begin{cases} 1 & \text{if } S(u, v) \leq S_0 \\ 0 & \text{otherwise} \end{cases} \quad (7)$$

where S_0 is the cutoff power spectrum level separating the wave numbers into two groups either with $S(u, v) > S_0$ or $< S_0$. The cutoff S_0 determined by means of S-A plot is such that distinct power-laws are observed between the distribution of power spectrum and the wave numbers (more about S-A method can be found Cheng et al., 2000). S-A method takes into account both anisotropic scale invariance of power spectrum and singularity in defining filter functions $H(u, v)$. The filter functions $H_B(u, v)$ and $H_A(u, v)$ generally correspond to low- and high-pass filters but they are fundamentally different from the commonly used frequency-based filters. The function $H_B(u, v)$ and $H_A(u, v)$ are not sharply bounded by range of frequency. These two types of filter functions can be used for separating anomalies from background for mineral exploration [11].



3.3 Experimental Procedure

For demonstration purposes we choose Zn concentration values as an example to implement the boundary-effect reduction method. Figure 4 shows the spatial distribution of Zn concentration values in the area denoting $f(x, y)$. For better understanding, a flowchart of the experimental procedure is given in

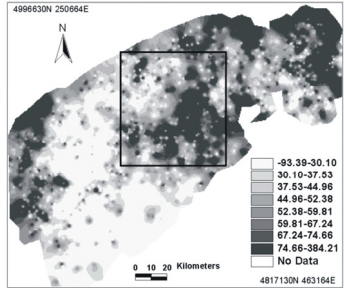


Figure 4. The spatial distribution of Zn element concentration in lake sediments, western Meguma Terrain, Nova Scotia, Canada.

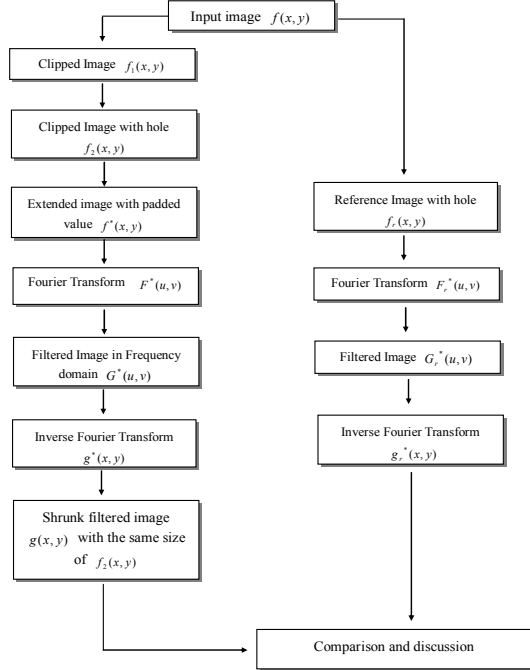


Figure 5. Flowchart of the experimental method.

Figure 5.

3.3.1 Input Image

To demonstrate the boundary effect problem, we clipped the central area of size 140×132 and with cell size 500m as highlighted by the rectangle in Figure 4. This will be used as the experimental data $f_1(x, y)$. Furthermore, in order to discuss the boundary effects of missing data, we artificially made a hole of size 14×15 in the input image $f_1(x, y)$ denoting it as $f_2(x, y)$. Figure 6 (A) and (B) show $f_2(x, y)$ and their corresponding power spectrum distributions, respectively. On these two images of power spectra we can clearly observe the bright cross along the axes that is due to the boundary truncations. The artificially made hole also creates the

high frequency noise on the power spectrum image. The high frequency noise has to be removed prior to further filtering.

3.3.2 Reference Image

To compare the results of boundary-effect correction using different methods and to assess the performances of different methods, it is convenient to define a reference image. Based on the preceding experimental data, we first calculate the power spectrum of an image, which denotes $f_r(x, y)$, clipped from the original image $f(x, y)$ around $f_1(x, y)$ with each side extended by 45 pixels. This treatment is needed in order to calculate a power spectrum close

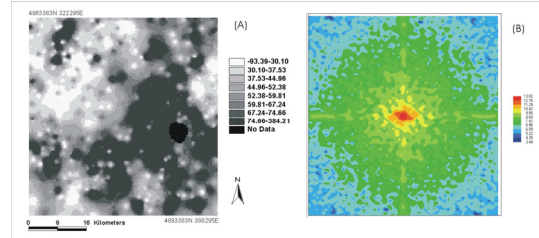


Figure 6. (A) Clipped small area from Figure 2 and artificially created hole in central area of map; and (B) power spectrum of image (A). The value is log-transformed (e based). It was calculated using fast Fourier transform in GeoDAS. to that of $f_1(x, y)$ with minimal boundary effects.

Applying the S-A method to the power spectrum produces the S-A plot on log-log paper shown in Figure 7. Different straight-line segments with different slopes represent different self-similarities, which usually correspond to different patterns in the spatial domain. For example, two straight-line segments were fitted to the data by least squares yielding a cutoff value $S_0 = 11.62$. The power spectrum $S < S_0$ may represent anomalies and the power spectrum $S > S_0$ usually corresponds to background [11]. For the current purpose, we are only interested in checking the anomalies in order to assess the boundary effects. Applying the high-frequency filter $H_A(u, v)$ defined in Eq. (7) with $S_0 = 11.62$ to the Fourier-transformed results and inverse Fourier

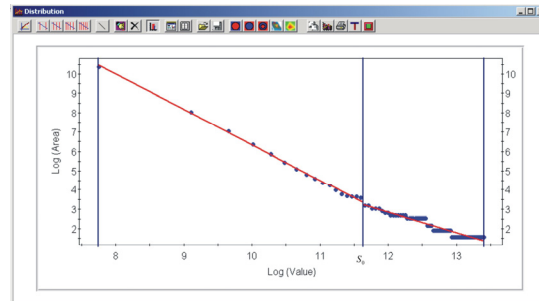


Figure 7. Log-log plot (S-A) showing the relationships between power spectrum value S and "area" $A(\geq S)$. Straight lines are fitted by means of LS. The power spectrum was calculated from an image clipped from the whole image $f(x, y)$ containing $f_1(x, y)$ but larger than $f_1(x, y)$ by 45 pixels around. Two straight line segments yield a cutoff value $S_0 = 11.62$. The details about how to determine breaks can be found from Cheng et al. (1999). The cutoff value will be used as threshold to construct filter $H_A(u, v)$ in Equation 5.



transform, the filtered image $g(x, y)$ can be generated.

As a result of the characteristics of the spatial distribution of the Zn concentration values used for the example, we can regard $g_c(x, y)$ as an ideal filtered image, which means $g_c(x, y)$ is free of boundary effects, clipped from $g(x, y)$. The size and spatial position of $g_c(x, y)$ are completely the same as those of $f_1(x, y)$. In order to compare the results with objectivity, we artificially clipped a hole in the image $g_c(x, y)$ with the same size and position as the hole in $f_2(x, y)$. This image with the hole, which is illustrated in Figure 8, was called $g_r(x, y)$ as the reference image of the input image $f_2(x, y)$.

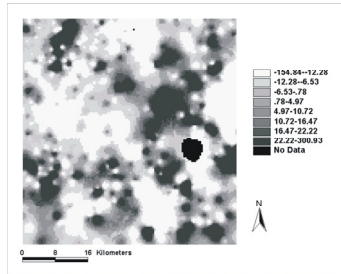


Figure 8. The reference image which was obtained using inverse Fourier transform with $H_A(u, v)$ applied. It was clipped according to the extent of $f_1(x, y)$ for further comparison purpose.

3.4 Comparison of Performance of Zero-padding and Decay Functions

In this experiment, we compare the performances of two methods, Zero-padding and Decay Functions, in reducing edge effects. For analyzing the reduction of edge effects with different extended portion Δ in each method, we set Δ ranging from 5 to 45 pixels with an interval of 10 pixels. The patterns in figure 4 show low values in boundary areas, but are high in the central area, so we select hyperbolic decay function. In figure 9, we describe the extended images with Δ from 5 (case A), 15(case B), 25 (case C), 35 (case D) and 45 (case E). We can compare these images with Figure 6 (A) and observe the change of extension part and hole in these images.

The results of filtered images obtained using zero-padding and hyperbolic decay function methods with the similar S_0 determined in comparison with S-A plot in Figure 7 are presented in Figures 10 and 11 respectively. Since the difference between the two distinct power-law relationships fitted to the S-A plot (Figure 7) is related to the actual different patterns (anomalous and background values), the slope distinction between these two power-law relationships is relatively independent of the edge effects. Experiments using $f_1(x, y)$ with various expansions have demonstrated that the scaling break (slope change between different power-law relationships) stays relatively unchanged. In this example, we adopt high frequency filters (see Equation 7) with the

predetermined value of S_0 . The results obtained with the filters are shown in Figures 10 and 11, respectively. By visual comparison of the results with the reference result in Figure 8, we can conclude intuitively that the decay function method overall provides results superior to zero-padding method. In particular, the decay function method provides

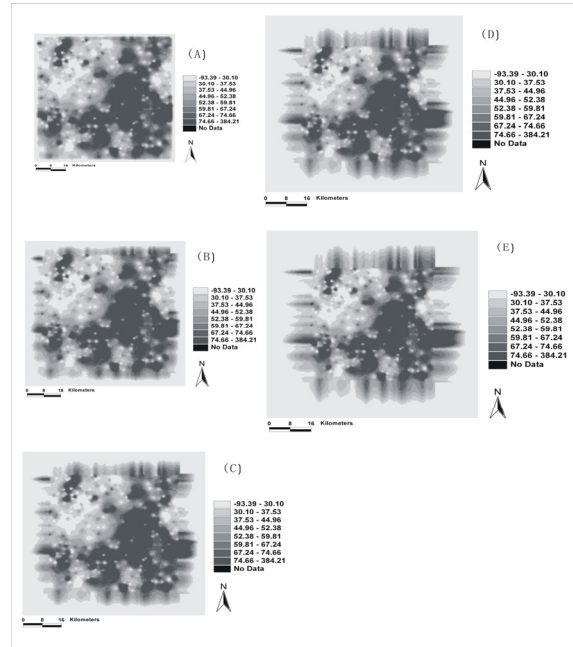


Figure 9. The extended images with Δ from 5 (case A), 15(case B), 25 (case C), 35 (case D) and 45 (case E)

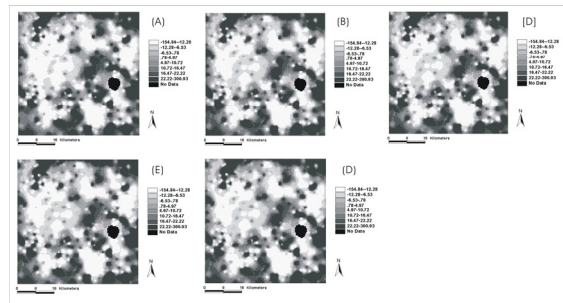


Figure 10. Filtered results obtained with high frequency filters using the zero-padding boundary effect correction method; (A)-(E) zero padding with extended widths $\Delta = 5, 15, \dots, 45$ pixel, respectively.

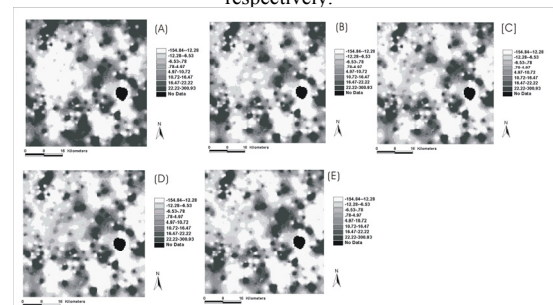


Figure 11. Filtered results obtained with high frequency filters using the Hyperbolic Decay Function; (A)-(E) Hyperbolic Decay Function with extended widths $\Delta = 5, 15, \dots, 45$ pixel, respectively.

satisfactory results for reducing the edge effects of holes.



4. Case Two: A Remote Sensing Imagery

In order to further substantiate the conceptual arguments, remotely sensed data was exemplified. In this case, reducing boundary effect is accompanied with the process of extracting ocean eddies from remotely sensed data using multifractal filtering function.

4.1 Study Area

This remotely sensed data is chosen from NASA MODIS as seen in Figure 12, which is located from 34°N-42°N, 66° W-78°W in the Gulf Stream. The size of SST image is 359 x 425 and cell size is 1000m and the SST image was acquired on June 21, 2004.



Figure 12 the study area chosen from NASA MODIS (satellite data set)

4.2 Implementation of Zero-padding and Decay Functions

Based on the self-similar and scale invariant properties of ocean eddies, we used S-A extract ocean eddies from remotely sensed data. Since the noise due to the boundary effect will affect subsequent operations such as frequency filtering, it is essential to eliminate boundary effects as much as possible. In this example, we still use decay function to reduce the boundary effect.

Applying the S-A method to this image to extract ocean eddies from remotely sensed data, we get the breaks like Figure 13. The segment between the second and the third straight lines would be the spectrum information of ocean eddies. The process of determining which segment represent the spectrum information of ocean eddies is tentative. The values of spectrum show in the table in the top right of Figure 13. From Figure 13, we can see that ocean eddies lie neither within high frequency region nor within low frequency region, is within middle frequency region. So we select band-pass filter to get the spectrum information of ocean eddies in frequency domain. Given the expanded image $f^*(x, y)$, we can apply S-A filtering method to get information of ocean eddies in frequency domain. Through inverse DFT⁻¹, the filtered image, ocean eddies in space domain, is obtained. The results from S-A equipped with the zero-padding and hyperbolic decay function are presented in Figures 14 and 15. The boundary effect on extracted patterns is reduced greatly in Figure 15, especially around boundary areas.

5. Conclusion

We have proposed an algorithm of using decay functions to smooth the boundaries of the image. The algorithm is particularly advantageous to deal with irregularly shaped images and those with missing data (holes). The implementation of the reduction of boundary effect using decay functions has been elaborated. Two case studies of filtering an image

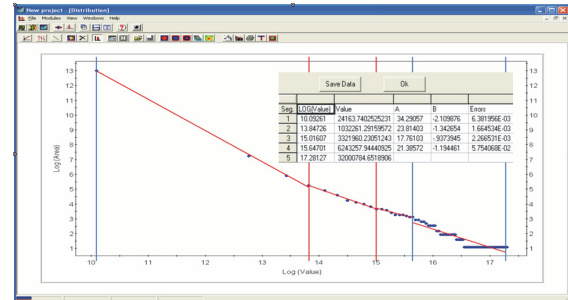


Figure 13 Log-log plot (S-A) showing relationships between power spectrum value S and "area" A (A ≥ S). Straight lines are fitted by means of least squares.

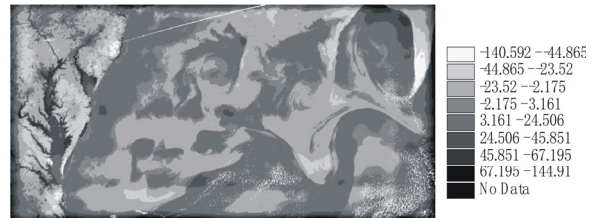


Figure 14 Ocean eddies extracted by S-A

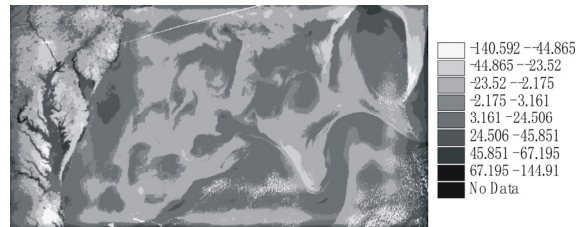


Figure 15 Ocean eddies extracted by S-A with the reduction of edge effect

created from lake sediment geochemical data and a remotely sensed imagery have demonstrated that S-A filtering method equipped with the boundary effect correction treatment significantly improves the filtering results. The performance of the decay function method has been shown to be superior in comparison with the zero-padding method. Issues worthy of further investigation include comparison of different decay functions on the reduction of boundary effects. Different detection technique for judge points, isolated points, boundaries/edges points need to be further investigated[13]. Other filters such as Wavelet and Gabour filter should be further tested to demonstrate the reduction of boundary effects.



6. Acknowledgements

The work is supported in part by Innovation Grant of Chinese Academy of Sciences (V36400) and OMET Grant P01-02-018 (Canada). The authors greatly appreciate their supports. The authors would like to thank Prof. Jan Flusser in Department of Image Processing, Institute of Information Theory and Automation Academy of Sciences of the Czech Republic for providing helpful comments for this research and Dr. Qingmou Li of Department of Earth and Space Science, York University for providing constructive suggestions about decay functions.

7. References

- [1] R. C. Gonzalez, R. E. Woods. Digital image processing. Upper Saddle River, N.J.: Prentice Hall, 793pp, 2002.
- [2] H. Radim. Boundary Effect Removing in Fourier Spectrum.
http://www.utia.cas.cz/user_data/scientific/ZOI_dept/image.html, 2005.
- [3] R. P. Haining. Spatial Data Analysis: Theory and Practice. University of Cambridge, 2003.
- [4] Li, Q.M., Cheng, Q.M., 2004. Fractal singular-value (Eigen-value) decomposition method for geophysical and geochemical anomaly reconstruction. Earth Science, a Chinese Journal of China University of Geosciences, 29(1), 109-118.
- [5] Y. Ge, Q. Cheng, S. Zhang. The Edge Effect Correction in S-A Method for Geochemical Anomaly Separation in GIS Environments, GeoTech Conference, Toronto, March, 2004.
- [6] J.W. Woods, J. Biemond, A.M. Tekalp. Boundary value problem in image restoration. Proceeding of Sixth International Conference, Acoustic Speech Signal Processing, pp.18.11.1-18.11.4, 1985.
- [7] A.M. Tekalp, M.L. Sezan. Quantitative analysis of artefacts in linear space-invariant image restoration. Multidimensional System Signal Processing, 1: 143-177, 1990.
- [8] H.C. Tan, H. Lim, B.T.G. Tan. 1991. Windowing techniques for image restoration. CVGIP: Graphical Models Image Processing, 53(5): 491-500, 1991.
- [9] D. W. Scott. Multivariate Density Estimation: Theory, Practice and Visualization. New York, J. Wiley, 1992.
- [10] F. Aghdasi, R.K. Ward. Reduction of boundary artifacts in image restoration. IEEE Transactions on Image Processing, 5(4): 611-618, 1996.
- [11] Q. M. Cheng, Y. G. Xu, E. Grunsky. Multifractal power spectrum-area method for geochemical anomaly separation. Natural Resources Research, 9(1): 43-51, 2000.
- [12] Q. M. Cheng. GeoData Analysis System (GeoDAS) for Mineral Exploration: User's Guide and Exercise Manual. Material for the training workshop on GeoDAS held at

Geological Survey of Canada, Ottawa, Dec. 9 to 11, 230p. www.gisworld.org/geodas, 2004.

- [13] D. Q. Chen, A. A. Farag, "Detecting Critical Points of Skeletons Using Triangle Decomposition of Gradient Vector Flow Field," The international journal of graphics, vision, and image processing (GVIP), 2006, Special Issue on Medical Image Processing.



Yong Ge was born on October 28, 1972 in P.R.China. She received the B.S. degree on surveying and mapping from Wuhan University, Wuhan, PRC, in 1995, the M.S. degree in geographical information system from the Wuhan university, Wuhan, PRC, in 1998, and the Ph.D. degree in cartography and geographical information system from Chinese Academy of Sciences in 2001. Since July 2001, she has been with the State Key Laboratory of Resources and Environmental Information System, Institute of Geographic Sciences and Natural Resources Research, Chinese Academy of Sciences where she is currently associate professor.



Qiuming Cheng was born on March 15, 1960 in P.R.China. He received the Ph.D. degree in earth science from University of Ottawa, Canada, in 1994. He is currently Professor in Department of Earth and Atmospheric Science and Department of Geography, York University, Canada and served as Director of CFI Geomatics Research Lab in York University. He is the recipient for a numbers of prestigious awards including President Prize by International Association for Mathematical Geology (IAMG), 1995; Canada Foundation for Innovation Researcher (CFI), 1998; Ontario Primer Research Excellent Award (PREA), 2000; and Foreign Researcher by Japan Society for the Promotion of Science (JSPS), 2002. He has served as Associate Editor, Computers & Geosciences, Editorial Board Member of Mathematical Geology, Geochemistry: Exploration, Environment and Analysis, Int. Journal of Ocean and Oceanography, Journal of Geophysics Progress and Journal of Earth Science, Fellow of Geological Association of Canada/Mineralogy Association of Canada (GAC), Fellow of International Association of Applied Geochemist (AEG), Council Member of International Association for Mathematical Geology (IAMG) Member, European Geological Union (EGU) and Member of America Geophysical Union (AGU).

